Published in final edited form as:
Mol Carcinog. 2013 February ; 52(2): 118–133. doi:10.1002/mc.21835.

Bortezomib-Induced Sensitization of Malignant Human Glioma Cells to Vorinostat-Induced Apoptosis Depends on Reactive Oxygen Species Production, Mitochondrial Dysfunction, Noxa Upregulation, Mcl-1 Cleavage, and DNA Damage

Daniel R. Premkumar[1,2], **Esther P. Jane**[1,2], **Naomi R. Agostino**[1,2], **Joseph D. DiDomenico**[2], and **Ian F. Pollack**[1,2,3,*]

[1]Department of Neurosurgery, Children's Hospital of Pittsburgh, Pittsburgh, Pennsylvania

[2]University of Pittsburgh School of Medicine, Pittsburgh, Pennsylvania

[3]University of Pittsburgh Cancer Institute Brain Tumor Program, Pittsburgh, Pennsylvania

Abstract

Glioblastomas are invasive tumors with poor prognosis despite current therapies. Histone deacetylase inhibitors (HDACIs) represent a class of agents that can modulate gene expression to reduce tumor growth, and we and others have noted some antiglioma activity from HDACIs, such as vorinostat, although insufficient to warrant use as mono-therapy. We have recently demonstrated that proteasome inhibitors, such as bortezomib, dramatically sensitized highly resistant glioma cells to apoptosis induction, suggesting that proteasomal inhibition may be a promising combination strategy for glioma therapeutics. In this study, we examined whether bortezomib could enhance response to HDAC inhibition in glioma cells. Although primary cells from glioblastoma multiforme (GBM) patients and established glioma cell lines did not show significant induction of apoptosis with vorinostat treatment alone, the combination of vorino-stat plus bortezomib significantly enhanced apoptosis. The enhanced efficacy was due to proapoptotic mitochondrial injury and increased generation of reactive oxygen species. Our results also revealed that combination of bortezomib with vorinostat enhanced apoptosis by increasing Mcl-1 cleavage, Noxa upregulation, Bak and Bax activation, and cytochrome *c* release. Further downregulation of Mcl-1 using shRNA enhanced cell killing by the bortezomib/vorinostat combination. Vorinostat induced a rapid and sustained phosphorylation of histone H2AX in primary GBM and T98G cells, and this effect was significantly enhanced by co-administration of bortezomib. Vorinostat/bortezomib combination also induced Rad51 downregulation, which plays an important role in the synergistic enhancement of DNA damage and apoptosis. The significantly enhanced antitumor activity that results from the combination of bortezomib and HDACIs offers promise as a novel treatment for glioma patients.

[*]Correspondence to: Department of Neurosurgery, Children's Hospital of Pittsburgh, 4401 Penn Avenue, Pittsburgh, PA 15223.

Conflicts of interest: None.

Additional Supporting Information may be found in the online version of this article.

Keywords

bortezomib; vorinostat; glioma; synergy; apoptosis

INTRODUCTION

Glioblastomas are aggressive tumors that generally respond poorly to current therapy with surgery, radiation, and conventional chemotherapy [1]. Molecularly targeted agents hold significant promise as novel therapeutic adjuncts, but to date, single agent therapies have generally failed to achieve high rates of long-term disease control in most patients, owing to the involvement of multiple redundant pathways for promoting growth and survival signaling in these tumors. These observations have called attention to the need to construct rationally directed combination strategies to achieve meaningful antiglioma activity. Histone deacetylase inhibitors (HDACIs) represent a class of agents of interest in this regard, that block the actions of histone deacetylases, which regulate gene expression by removal of acetyl groups from specific lysine-rich amino terminal residues on nucleosomal histones [2], thus altering the balance between condensed and relaxed chromatin. Chromatin condensation due to high HDAC activity leads to transcriptional silencing of a subset of genes involved in differentiation and inhibition of proliferation, apoptosis, and metastasis [3]. HDACIs inhibit neoplastic cells through diverse mechanisms, including induction of oxidative injury [4], upregulation of death receptors, cell cycle checkpoint disruption [5], interference with HSP90 function [6], and upregulation of proapoptotic proteins [3,7]. Inhibition of reactive oxygen species (ROS) generation with ROS scavengers or forced overexpression of the Bcl-2 protein has been observed to protect AML cell lines from HDACI-induced apoptosis [8], suggesting that ROS may play an important mechanism in HDAC-mediated apoptosis. Suberoylanalide hydroxamic acid (SAHA, vorinostat), an inhibitor of several members of the HDAC protein family [9], has also been observed to have antiglioma activity by our group [10,11] and others in vitro and in orthotopic xenografts in vivo [12,13], although our studies indicated that the predominant effects were antiproliferative, rather than proapoptotic, at clinically achievable concentrations. We therefore questioned whether the therapeutic effects of vorinostat could be enhanced by combination with a second agent that promoted ROS release, thus enhancing induction of glioma cell apoptosis.

Proteasome inhibitors (PIs) represent a promising novel class of anticancer agents [14] that is already in clinical use, as bortezomib (PS-341/Velcade) has been approved for the treatment of multiple myeloma [15]. We have recently demonstrated that bortezomib exhibited potent antiglioma activity and dramatically sensitized even highly resistant glioma cells to TRAIL cytotoxicity, suggesting that proteasomal inhibition may be a promising combination strategy for glioma therapeutics [16]. Moreover, PIs have been observed to induce apoptosis in solid tumors, such as lung and prostate cancer [17,18], and several reports have shown that the combination of bortezomib and HDAC inhibition abrogates HSP90 chaperone function [6], and augments the cytotoxic effects of paclitaxel [19]. However, the possible effects and therapeutic mechanism of this combination in glioma cells remain undefined. In this study, we showed that, although vorinostat treatment alone did not

induce apoptosis in glioma cells at clinically achievable concentrations, this agent significantly enhanced bortezomib-induced apoptosis by activating proapoptotic mitochondrial injury and release of cytochrome *c*. Our results also revealed that co-treatment of bortezomib and HDACIs enhanced apoptosis by increasing Noxa and Mcl-1 cleavage. The significantly enhanced antitumor activity that results from the combination of bortezomib and HDACIs offers promise as a novel treatment for glioma patients.

MATERIALS AND METHODS

Cell Lines

Primary cultures were obtained from freshly resected tissues after surgical removal under an Institutional Review Board-approved protocol for acquisition and the use of tumor tissue collected at the time of tumor resection. We also obtained glioblastoma multiforme (GBM) primary cells from Conversant Biologics (Huntsville, AL), which were cultured in DMEM/F12 (Invitrogen, Carlsbad, CA). The established malignant glioma cell lines U87 (p53 wild type), T98G (p53 mutant), U373 (p53 mutant), LN229 (p53 mutant), and A172 (p53 wild type) were obtained from the American Type Culture Collection (Manassas, VA). LNZ308 (p53 deleted) was provided by Dr. Nicolas de Tribolet. T98G, U87, and U373 cell lines were cultured in growth medium composed of minimum essential medium; LN229, A172, and LNZ308 were cultured in α-minimal essential medium. All growth media contained 10% fetal calf serum, L-glutamine, 100 IU/mL penicillin, and 100 mg/mL streptomycin (Invitrogen) supplemented with sodium pyruvate and nonessential amino acids. Normal human astrocytes (NHA) and media were obtained from ScienCell Research Laboratories (San Diego, CA).

Reagents and Antibodies

Vorinostat and bortezomib were purchased from Chemie Tek (Indianapolis, IN). ROS indicator H_2DCFDA was purchased from Invitrogen and dissolved in DMSO. Free radical scavenger, *N*-acetyl-L-cysteine (NAC), was purchased from EMD Chemicals (Philadelphia, PA). Pancaspase inhibitor (Z-VAD-fmk) was purchased from R&D Systems (Minneapolis, MN). The following antibodies were used: Cytochrome *c* (#4280), Bim (#2819), Bcl-2 (#2872), Bcl-xL (#2764), Mcl-1 (#4572), Bak (3814), Bax (#2774), cleaved PARP (#9546), cleaved caspase 3 (#9664), cleaved caspase 9 (#9501), phospho-H2AX (#2577), and β-actin (#4970) were from Cell Signaling Technology, Inc. (Beverly, MA). Noxa (sc-26917) was from Santa Cruz Biotechnology, Inc. (Santa Cruz, CA). Monoclonal anti-Bax (#556467) was from BD Pharmingen (San Diego, CA), monoclonal anti-Bak (Ab-1, TC-100; #AM03) was from Calbiochem (EMD Chemicals, Philadelphia, PA), protocol for acquisition and RAD51 (ab63801) was from Abcam (Cambridge, MA).

Cell Proliferation and Cytotoxicity Assay

Cells (5×10^3/well) were plated in 96-well microtiter plates (Costar, Cambridge, MA) in 100 μL of growth medium, and after overnight attachment, exposed for 3 d to inhibitors or vehicle (DMSO). After the treatment interval, cells were washed in medium, and the number of viable cells was determined using a colorimetric cell proliferation assay (CellTiter96 Aqueous NonRadioactive Cell Proliferation Assay; Promega, Madison, WI) [20]. All studies

were conducted as previously described [16]. Morphological changes in response to inhibitor treatment were evaluated by microscopic inspection and imaging of cells using an Olympus FluoView 1000 microscope. Images were assembled using Adobe Photoshop CS2 software (Adobe Systems, Inc., New York, NY).

Clonogenic Growth Assay

The effect of inhibitor treatment on colony forming ability was assessed using a clonogenic assay. Two hundred and fifty cells were plated in six-well trays in growth medium, and after overnight attachment, exposed to inhibitors or vehicle for 1 d. Cells were then washed with inhibitor-free medium, grown for 2 wk under inhibitor-free conditions, and fixed and stained (Hema 3 Manual Staining Systems; Fisher Scientific, Pittsburgh, PA). Plates were then scanned and images were assembled using Adobe Photoshop CS2 software (Adobe Systems, Inc.).

Annexin V Apoptosis Assay

Apoptosis induction in vehicle- or inhibitor-treated cells was assayed by the detection of membrane externalization of phosphatidylserine using an Annexin V assay kit (Molecular Probes, Invitrogen, Carlsbad, CA) as described previously [16,21]. Cells (2×10^5) were harvested at various intervals after treatment, washed with ice-cold phosphate-buffered saline (PBS) and resuspended in 200 μL of binding buffer. Annexin V-FITC and 1 μg/mL propidium iodide were added and cells were incubated for 15 min in a dark environment. Labeling was analyzed by flow cytometry with a FACSCalibur flow cytometer (BD Biosciences, San Jose, CA).

Cell Cycle Analysis

The effect of varying concentrations of inhibitors on cell cycle distribution was determined by flow cytometric analysis of the nuclear DNA content as previously described [21]. Briefly, cells grown exponentially to 50–60% confluency were exposed to the inhibitors or DMSO for a range of intervals, harvested, washed in ice-cold PBS, and fixed in 70% ethanol. DNA was stained by incubating the cells in PBS containing propidium iodide (50 μg/mL) and RNase A (1 mg/mL) for 60 min at room temperature, and fluorescence was measured and analyzed using a Becton Dickinson FACScan and Cell Quest software (Becton Dickinson Immunocytometry Systems, San Jose, CA).

Subcellular Fractionation

Cells were treated with or without inhibitors and cytosolic proteins were fractionated as described by Nencioni et al. [22]. Briefly, cells were resuspended in a lysis buffer containing 0.025% digitonin, 250 mmol/L sucrose, 20 mmol/L HEPES (pH 7.4), 5 mmol/L $MgCl_2$, 10 mmol/L KCl, 1 mmol/L EDTA, 1 mmol/L phenylmethylsulfonyl fluoride, 10 μg/mL aprotinin, 10 μg/mL leupeptin. After 10-min incubation at 4°C, cells were centrifuged (2 min at 13 000*g*) and the supernatant (cytosolic fraction) was removed and frozen at −80°C for subsequent use. The resulting digitonin-insoluble pellet was further dissolved in 2% SDS buffer as a membrane-bound organellar fraction enriched with mitochondria. These two fractions were analyzed by immunoblotting. The distribution of heat shock protein 70

(HSP70) was used to determine that cytoplasmic cytochrome *c* did not result from mitochondria damaged in the course of the protocol.

DiOC6 Labeling and Detection of Mitochondrial Membrane Depolarization

Mitochondrial membrane depolarization was measured as described elsewhere [23]. In brief, floating cells were collected, and attached cells were trypsinized and resuspended in PBS. Cells were loaded with 50 nM 3′,3′-dihexyloxacarbo-cyanine iodide (DiOC6, Molecular Probes, Invitrogen) at 37°C for 15 min. The positively charged DiOC6 accumulates in intact mitochondria, whereas mitochondria with depolarized membranes accumulate less DiOC6. Cells were spun at 3000*g*, and rinsed with PBS twice and resuspended in 1 mL of PBS. Fluorescence intensity was detected by flow cytometry and analyzed with CellQuest software (Becton Dickinson, San Jose, CA). The percentage of cells with decreased fluorescence was determined.

Determination of Reactive Oxygen Species

ROS production was monitored with the cell-permeable ROS indicator, 2′,7′-dichlorodihydro-fluorescein diacetate (H_2DCFDA) (Invitrogen), as described by Cossarizza et al. [24]. After treatment, cells were washed with PBS, incubated with 5 μM H_2DCFDA for 30 min, and washed again with PBS. Fluorescence intensity was measured by flow cytometry (Becton Dickinson). This dye (H_2DCFDA) is a cell-permeable molecule, which is very sensitive to intracellular redox change [24]. The functional role of ROS generation on apoptosis was assessed in additional experiments using the free radical scavenger NAC. Cells were preincubated with 5 mM NAC for 2 h, followed by co-incubation with inhibitors and assessment of apoptosis or ROS generation as described above.

Immunoprecipitation and Western Blotting Analysis

Treated and untreated cells were washed in cold PBS and lysed in buffer containing 30 mM HEPES, 10% glycerol, 1% Triton X-100, 100 mM NaCl, 10 mM $MgCl_2$, 5 mM EDTA, 2 mM Na_3VO_4, 2 mM β-glycerophosphate, 1 mM phenylmethylsulfonyl fluoride, 1 mM 4-(2-aminoethyl) benzenesulfonyl fluoride, 0.8 μM aprotinin, 50 μM bestatin, 15 μM E-64, 20 μM leupeptin, and 10 μM pepstatin A for 15 min on ice. Samples were centrifuged at 12 000*g* for 15 min, supernatants were isolated, and protein was quantified using Protein Assay Reagent (Pierce Chemical, Rockford, IL). Equal amounts of protein were separated by SDS–poly-acrylamide gel electrophoresis (PAGE) and electro-transferred onto a nylon membrane (Invitrogen). Nonspecific antibody binding was blocked by incubation of the blots with 4% bovine serum albumin in Tris-buffered saline (TBS)/Tween 20 (0.1%) for 1 h at room temperature. The blots were then probed with appropriate dilutions of primary antibody overnight at 4°C. The antibody-labeled blots were washed three times in TBS/Tween 20 for 15 min and then incubated with a 1:2000 dilution of horseradish peroxidase-conjugated secondary antibody (Santa Cruz Biotechnology, Inc.) in TBS/Tween 20 at room temperature for 1 h. After additional washing in TBS/Tween 20, the proteins were visualized by Western Blot Chemiluminescence Reagent (Cell Signaling Technology, Inc.). Where indicated, the blots were reprobed with antibodies against β-actin to ensure equal loading and transfer of proteins.

For immunoprecipitation, cell extracts were prepared by lysing 5×10^6 cells on ice for 30 min in CHAPS lysis buffer (10 mM HEPES (pH 7.4), 137 mM NaCl, 2 mM EDTA, 2% CHAPS, protease, phosphatase inhibitors). Lysates were clarified by centrifugation at 15 000*g* for 10 min at 4°C, and the protein concentrations in the supernatants were determined. Equal amounts of protein extracts were incubated overnight with primary antibody. Afterward, Dynabeads Protein G (Invitrogen) was added for 2 h. Supernatant (non-immunoprecipitated fraction) was recovered by magnetic separation, and G-protein beads (immunoprecipitated fraction) were washed with ice cold CHAPS lysis buffer and Western blot analysis was carried out as described above. Scanning densitometry was done on Western blots using acquisition into Adobe Photoshop (Adobe Systems, Inc.) followed by image analysis (UN-SCAN-IT gel, version 6.1; Silk Scientific).

Transient Transfection

Optimal 29mer-pRS-shRNA constructs were obtained from Origene (Rockville, MD). Sequences specific for human Mcl-1 (ACC TAG AAG GTG GCA TCA GGA ATG TGC TG), Noxa (GGA GGT GCT ACA CAA TGT GGC GTC GGC AC) and control sequences (GCA CTA CCA GAG CTA ACT CAG ATA GTA CT) (non-target shRNA) were used for this study. Glioma cells were seeded in six-well plates and allowed to reach 70–80% confluence. Transfection of targeting or control (non-targeting) shRNA was performed by using FuGene 6 according to the manufacturer's recommendations (Roche Applied Science, Indianapolis, IN). One microgram of Mcl-1, Noxa or non-targeting shRNA in 100 μL Opti-MEM medium was mixed with 2 μL of FuGene 6. After the mixture was incubated at room temperature for 20 min, complete medium was added to make the total volume up to 2 mL. After 48 h, media were changed and cells were incubated with inhibitors for 24 h. Cell viability (annexin V binding) or Western blot analysis were carried out as described above.

Immunocytochemistry and Fluorescence Microscopy

Cells were grown on chamber slides (Nalge Nunc, Naperville, IL) in growth medium, and, after an overnight attachment period, were exposed to selected concentrations of inhibitor or vehicle (DMSO) for various intervals. Cells were washed once with PBS, fixed with 3.7% formaldehyde for 30 min, washed two times in PBS, and then per-meabilized with 0.1% Triton X-100 in PBS for 10 min. Cells were washed with PBS, blocked with 0.5% bovine serum albumin for 1 h and then incubated with primary antibodies overnight at 4°C. After PBS wash, the slides were incubated with secondary antibody and Hoechst 33342 (Invitrogen) for 2 h at room temperature. The slides were then washed in PBS, mounted, and examined under a fluorescent microscope.

Combination Index Analysis

Logarithmically growing glioma cells were seeded in 96-well microplates at 5000 cells/well and were allowed to attach overnight. Cells were treated with increasing concentrations of single-agent bortezomib, vorinostat, or the combination in a fixed concentration ratio [bortezomib/vorinostat (1:500)]. Control cells received DMSO. Cell viability was measured using MTS cell proliferation assay as described above. The dose–effect curve parameters for both bortezomib and vorinostat were used for the calculation of the combination index (CI)

by the Calcusyn software (BIOSOFT, Cambridge, UK) where CI values <1, =1, and >1 indicate synergism, additivity, and antagonism, respectively [25].

Statistical Analysis

Unless otherwise stated, data are expressed as mean ± SD. The significance of differences between experimental conditions was determined using a two-tailed Student's *t*-test. Differences were considered significant at *P* values <0.05.

RESULTS

Bortezomib Sensitizes Glioma Cells to Vorinostat

Previously we examined the independent effect of three different HDACIs, vorinostat, trichostatin A (TSA), and sodium butyrate, on the cytotoxicity of established glioma cell lines [10,11]. Statistically significant inhibition of cell proliferation was detectable in all tested cell lines in a p53-independent manner. Additionally, vorinostat was shown to sensitize glioma cells to apoptosis induced by vandetanib [10]. In this report, we sought to determine whether the antiproliferative activity induced on glioma cell lines by HDACIs was caused by cell-cycle arrest and/or induction of programmed cell death. To test that, clonogenic growth assay and annexin V staining-based flow-cytometry evaluation were used. Cells were incubated with either medium or vorinostat for 24 h (clonogenic growth assay) or 72 h (annexin V evaluation). No significant difference in the colony forming ability was observed between untreated and treated cells after 24 h treatment (Figure 1A). With longer exposure times at concentrations above the clinically achievable range, modest cytotoxicity with vorinostat was evident in primary GBM cells and the T98G glioma cell line. Interestingly, vorinostat had little or no effect on non-neoplastic human astrocytes (NHA), even at higher concentrations, suggesting that vorinostat acts selectively against glioma cells versus non-neoplastic astrocytes (Supplementary Figure 1). Nonetheless, cell cycle analysis shows that vorinostat affected cell cycle progression, as manifested by cell accumulation at G_2M phase (Figure 1B), but not the frequency of cells with sub-G_1 DNA content, which is consistent with Annexin V and clonogenic assays (Figure 1A and Supplementary Figure 1).

Other investigators have shown that co-administration of HDAC inhibitors with PIs induces a marked increase in apoptosis in retinoblastoma [26], myeloma [27], and lymphoma [28]. To understand the precise mechanism and to gain further insight into the interactions in glioma, median dose–effect isobologram analysis was performed as described by Chou and Talalay [25]. For bortezomib and vorinostat, the combination index values were <1.0 in all glioma cell lines. The combination index values were 0.65, 0.55, 0.48, 0.51, 0.41, and 0.56 for U87, T98G, U373, A172, LN229, and LNZ308, respectively. To investigate the potential of bortezomib to sensitize glioma cells to vorinostat, we then examined the effect of bortezomib alone or in combination with vorinostat in primary tumor cells isolated from surgical specimens, established glioma cell lines, and non-neoplastic human astrocytes (NHA). Colony forming ability and apoptotic cell death was determined by clonogenic growth assay (Figure 1C), and by annexin V binding at the cell surface (Figure 1D) and Western blot analysis (Figure 1E), respectively. Neither bortezomib nor vorinostat alone

resulted in a significant reduction of viable cells; however, combining bortezomib with vorinostat significantly inhibited the colony forming ability in established glioma cell lines (Figure 1C). In addition, simultaneous treatment with bortezomib and vorinostat resulted in a significant increase of cell death as measured by annexin V binding (Figure 1D) and cleavage of PARP (Figure 1E) in established glioma cell lines and primary GBM cells, but not in non-neoplastic human astrocytes (NHA). Further, cell cycle profiling showed that the combination of vorinostat and bortezomib increased the fraction of sub-G_1 apoptotic cells from <10% (vorinostat alone) to 25–40% (vorinostat and bortezomib) in T98G and primary GBM cells, respectively (Figure 1F). Together, these findings demonstrate that vorinostat induces G_2M cell cycle arrest and produces minimal or no apoptotic cell death in malignant human glioma cell lines at clinically achievable concentrations, whereas combined inhibition of proteasome activity markedly increases the sensitivity of glioma cells to vorinostat.

Combination of Bortezomib and Vorinostat Induces Loss of Mitochondrial Potential and Release of ROS

Because bortezomib induces mitochondrial membrane potential ($\Delta\psi_m$) dissipation as a mechanism for promoting apoptosis [16], and mitochondrial changes are necessary for the activation of downstream caspases [22], we investigated the combined effect of bortezomib and vorinostat on mitochondrial membrane potential. The mitochondrial uncoupler, CCCP, was used as a positive control for $\Delta\psi_m$ disruption. As shown in Figure 2A and B, bortezomib induced loss of $\Delta\psi_m$ in a dose-dependent manner in primary and established glioma cells as evidenced by the appearance of a subpopulation of cells with reduced $\Delta\psi_m$ (Figure 2). In addition, combination of bortezomib and vorinostat induced a strong increase in the loss of mitochondrial membrane depolarization (Figure 2C).

ROS generation following HDAC inhibitor treatment has been described by several groups in several different cell line systems [4,29]. Because production of ROS following MS-275 administration [29] and induction of cell death resulting from proteasome inhibition was linked to increased levels of ROS in leukemia cells [30], experiments were carried out to measure the capacity of proteosomal inhibition to modulate intracellular ROS content in glioma cells. Not surprisingly, bortezomib induced ROS accumulation in a dose-dependent manner in primary GBM (Figure 2D, left panel) as measured by the ROS indicator H_2DCFDA. Combination of bortezomib (5 nM) with vorinostat (2 μM), further enhanced ROS generation (Figure 2D, right panel). Similar ROS activation was seen in glioma cell lines (e.g., T98G, U87, and LN229) with the combination of bortezomib and vorinostat (data not shown).

Taken together, when used in combination, vorinostat and bortezomib greatly cooperated to induce apoptosis, as manifested by sub-G_1 DNA content (Figure 1F), and cell surface annexin V binding (Figure 1D), and to reduce cell viability as manifested by MTS assay (data not shown). Pre-treating cells with the pancaspase inhibitor Z-VAD-fmk and the free radical scavenger NAC greatly reduced the bortezomib + vorinostat-induced apoptotic cells (Figure 2E, left panel), which indicates that the observed cell death is a caspase-dependent process. Moreover, $\Delta\psi_m$ reduction appeared as a caspase-dependent response, which was

prevented by the pancaspase inhibitor Z-VAD-fmk (Figure 2E, right panel). The importance of ROS production by vorinostat + bortezomib-provoked apoptosis potentiation was proved using the free radical scavenger, NAC. For example, pretreating cells with NAC greatly attenuated apoptosis generation (Figure 2E, left panel) and $\Delta\psi_m$ dissipation (Figure 2E, right panel). These results indicated that the interaction between the two stimuli is apparent at the level of the mitochondria, which may play an important role in promoting synergistic apoptosis induction.

Co-treatment With Bortezomib and Vorinostat Induces Bak and Bax Conformational Changes and Cytochrome *c* Release

Among the members of the Bcl-2 family, the multidomain proteins Bax and Bak are crucial for the activation of mitochondria. Several reports have demonstrated that generation of ROS [31] as well as the loss of $\Delta\psi_m$ [32] plays a critical role in the regulation of Bax and Bak. We [33] and others [32] have reported that Bax and Bak protein conformation changes are necessary steps in cells undergoing apoptosis. To address the potential contribution of Bax and Bak alterations to the combined effects of bortezomib and vorinostat, cells were exposed to both agents, alone or in combination, for 24 h and the conformational status of Bak and Bax was assessed by flow cytometry and immunoprecipitation analysis. Bak and Bax antibodies that recognize their active conformations were used in order to investigate Bak and Bax involvement in the combination of bortezomib and vorinostat-induced apoptosis (Figure 3A). Treatment of T98G cells with vorinostat (2 μM) or bortezomib (5 nM) induced a minimal or no activation of Bak or Bax (Figure 3A). However, the combination of both for 24 h induced an increased activation of both Bak and Bax (Figure 3A). Bak and Bax activation was seen also in similarly treated primary GBM cells at 24 h with the combination of bortezomib and vorinostat (data not shown). To further validate these observations, cell lysates were immunoprecipitated with anti-BAX 6A7 or anti-BAK (Ab-1) antibodies and active Bax and Bak protein levels were detected by Western blot analysis. As shown in Figure 3B, the signal of active Bax and Bak was barely detectable in untreated control cells or with single agent treatment, whereas activated Bax and Bak increased significantly in lysates extracted from cells treated with the combination of vorinostat and bortezomib. Pretreating cells with Z-VAD-fmk or NAC blocked bortezomib and vorinostat-induced Bak and Bax activation (Figure 3C), suggesting that caspases and generation of ROS plays a major role in Bak and Bax activation in malignant human glioma cells.

Bak and Bax activation is associated with the permeabilization of mitochondrial membranes and cytochrome *c* release [34]. Vander Heiden et al. [35] provided evidence that during apoptosis there is a disruption of mitochondrial membrane potential, which may be responsible for the release of cytochrome *c*. Because caspases and mitochondria can engage in a self-amplification loop in which the release of mitochondrial apoptogenic proteins activates caspases that would in turn increase the mitochondrial membrane permeability [36], and the combination of bortezomib and vorinostat was promoting mitochondrially mediated apoptotic signaling, we examined the release of cytochrome *c* to the cytosol after inhibitor treatment, alone or in combination. As shown in Figure 3D, the signal of cytochrome *c* was barely detectable in cytosol when the cells incubated with bortezomib or

vorinostat alone, but clearly detected with the combination of bortezomib and vorinostat. Under the same conditions, we also detected the release of Smac/DIABLO, another apoptotic regulator, with a similar pattern to that of cytochrome *c* release (data not shown). Taken together, we propose that co-treatment with bortezomib and vorinostat activates Bak and Bax, and releases proapoptotic factors including cytochrome *c* that is needed to activate caspases [37].

Co-treatment With Vorinostat and Bortezomib Triggers Accumulation of Bim, Noxa, and Mcl-1 Cleaved Fragments and Disrupts Mcl-1/Bim Complexes in Malignant Human Glioma Cells

Recently we have shown that the expression of Mcl-1 and p21 was significantly enhanced by bortezomib [16]. To characterize the interactions between vorinostat and bortezomib, cells were incubated with vorinostat with or without bortezomib for the indicated durations. As shown in Figure 4A, treatments with these inhibitors caused no effect on Bcl-2 and Bcl-xL expression. No significant changes were observed in Bad or Bik in all cell lines tested (data not shown). However, combination of vorinostat with bortezomib treatment significantly increased the expression of Bim (particularly the BimL and BimS isoforms), Noxa and the cleaved forms of Mcl-1 (Figure 4A). In untreated cells, Bim was predominantly co-immunoprecipitated by Mcl-1, Bcl-xL and by Bcl-2. Cells exposed to bortezomib and vorinostat clearly demonstrate the release of BimL or BimS from binding by Mcl-1, Bcl-2 and to a lesser extent by Bcl-xL (Figure 4B). Noxa is a BH3 domain only, proapoptotic, Bcl-2 family member and is known to potently bind and inhibit Mcl-1 [38]. Then to address the role of Noxa and Mcl-1, immunoprecipitation using anti-Mcl-1 antibody followed by Western blotting was carried out using cells treated with inhibitors alone or in combination. An increased Mcl-1–Noxa complex was detected after bortezomib and HDACI treatment whereas Mcl-1–Bim complexes were reduced, suggesting the disruption of Mcl-1–Bim complexes (Figure 4C) after inhibitor treatment, supporting the notion that Noxa acts as a major proapoptotic protein by interacting with Mcl-1 [38,39]. Further, pretreating cells with Z-VAD-fmk and NAC resulted in a significant inhibition of active caspase-9, active caspase-3 and PARP (Figure 4D), accompanied by reduction in levels of Mcl-1 (cleaved form) (Figure 4D). Together, these results indicate that upregulation of Noxa is at least partially responsible for mediating glioma cell death by synergistic combinations of vorinostat and bortezomib.

Knocking Down Mcl-1 Expression Increases Glioma Cell Sensitivity to Bortezomib and Vorinostat and Knocking Down Noxa Expression Protects Cells From Killing Induced by the Combination of Bortezomib and Vorinostat

As proapoptotic Noxa mainly binds to the antiapoptotic protein Mcl-1, we investigated the biological relevance of our observed Mcl-1 cleavage and Noxa induction by knocking down Mcl-1 or Noxa using RNA interference. Immunoblot analysis indicated that Mcl-1 shRNA versus non-target shRNA inhibited bortezomib-induced Mcl-1 protein expression by ~60–85% (Figure 5A, left panel). However, when the cells were treated with bortezomib or vorinostat or the combination of both, blocking Mcl-1 expression by Mcl-1 shRNA significantly increased Annexin V positive cells (Figure 5B). These results demonstrate that Mcl-1 mediates resistance to bortezomib and vorinostat.

To investigate the involvement of Noxa, T98G cells were transiently transfected with Noxa shRNA. Western blot analysis indicated that Noxa shRNA versus non-target shRNA significantly inhibited bortezomib-induced Noxa protein expression (Figure 5A, right panel). In parallel, when cells were treated with bortezomib and vorinostat, blocking Noxa expression significantly decreased apoptotic cells (Figure 5B).

Vorinostat and Bortezomib Provoke DNA Damage Response in Malignant Human Glioma Cell Lines

Other authors have demonstrated previously that glioma cell lines express high Rad51 protein levels and that they can be radiosensitized by targeting Rad 51-dependent repair [40], antisense targeting Rad51 [41], Gleevec [42], or vorinostat [43]. Because vorinostat has been observed to abrogate key DNA damage repair processes and attenuate prosurvival signals, thereby conferring radiosensitivity to glioma cells [43], we examined the effect of vorinostat treatment with or without bortezomib on the expression of proteins known to be involved in the repair of double-strand breaks and other repair processes. Immunofluorescence and immunoblot analyses of the phosphorylation of histone H2AX on Ser139, a surrogate marker of DNA double strand breaks (DSB) [44] and expression of Rad51 levels were analyzed. Vorinostat and bortezomib induced a rapid and sustained phosphorylation of histone H2AX on Ser139 in primary GBM and T98G cells, and this effect was significantly enhanced by co-administration of the two agents (Figure 6A), whereas the combination of bortezomib and vorinostat induced Rad51 downregulation. Immuno-fluorescence studies revealed the formation of γ-H2AX foci in glioma cells as early as 3 h. This elevated level of expression was maintained for up to 48 h after inhibitor treatment (Figure 6B, upper panel). Conversely, the expression of RAD51 was significantly diminished after 12 h of exposure to bortezomib and vorinostat (Figure 6B, lower panel). This prolongation of γ-H2AX foci levels following the combination compared with controls suggests that the combination of bortezomib and vorinostat inhibits the repair of DNA damage. In parallel, we tested the effects of the pan caspase inhibitor Z-VAD-fmk and the free radical scavenger NAC on bortezomib + vorinostat-induced modulation of Rad51 and pH2AX. As shown in Figure 6C, pretreating cells with Z-VAD-fmk significantly inhibited bortezomib and vorinostat-induced H2AX phosphorylation (~80% inhibition) and Rad51 downregulation was inhibited by 40%. Furthermore free radical scavenger, NAC, significantly inhibited bortezomib + vorinostat-induced pH2AX phosphorylation (~35%) and inhibited Rad51 downregulation by 50%, suggesting that ROS plays an integral role in the bortezomib and vorinostat-induced DNA damage pathway. Together, these results suggest that co-treatment with bortezomib and vorinostat can not only induce DSB (as evidence by H2AX activation), but also block DNA double-strand break homologous recombination repair (due to downregulation of Rad51), which could represent an additional mechanism underlying the significant sensitizing effects observed with this combination in glioma.

DISCUSSION

The HDACIs are promising anticancer drugs that may selectively induce differentiation and cell death of certain transformed cells versus their normal counterparts, and inhibit proliferation of others. Members of this class of agents are now under clinical trials for both

hematological and solid tumors [45] including glioma [46]. Our previous studies have indicated that the predominant effects of HDACIs in glioma cell lines in vitro are cytostatic rather than cytotoxic, which fits with the relatively modest effects that have been observed in glioma clinical trials with HDACIs, such as vorinostat. We have also observed that proteasomal inhibitors may promote a more proapoptotic milieu [16,47] in gliomas, and render even highly apoptosis-resistance cells more sensitive to induction of apoptotic signaling. In this study, we examined the effect of simultaneous inhibition of HDAC and proteasomes on glioma growth and survival. The effects observed with the combination differ substantially from the effects seen in glioma cells treated with vorinostat or bortezomib alone. Our results demonstrate a striking potentiation of apoptosis induction with this combination that far exceeds the effects with either inhibitor alone. p53 mutations are among the most common glioma genetic alterations, and p53-mutated glioma cell lines are generally more chemoresistant [48]. It is pertinent that no significant vorinostat [10] or bortezomib [16] response differences were seen in p53-wild type (A172), mutated (T98G), or deleted (LNZ308) glioma cells. When administered as single agents at clinically achievable concentrations, vorinostat inhibited the growth of glioma cells in a dose-dependent and p53-independent manner [10–12], but produced minimal or no apoptotic cell death in primary and established human glioma cell lines. In contrast, we found that the combination of vorinostat and bortezomib had a synergistic cytotoxic effect in vitro in a p53-independent manner.

TThe mode of apoptosis induction by the vorinostat and bortezomib combination involved activation of intrinsic (mitochondrial) caspase pathways. This effect is characterized by a marked enhancement in mitochondrially mediated apoptotic signaling as demonstrated by loss of mitochondrial membrane potential ($\Delta\psi_m$), increased generation of ROS, and release of cytochrome *c* into the cytosol. This ROS production, as well as concomitant cell death, was blocked by co-incubation with the free radical scavenger NAC. We noted that ROS production likely represents a significant mode of action of bortezomib and vorinostat in glioma cells. Compared with the limited effects observed with single agent therapy, addition of bortezomib together with vorinostat triggered the release of the proapoptotic protein cytochrome *c* into the cytosolic fraction and accumulation of increased levels of cleaved caspases and PARP, hallmarks of apoptosis. Consistent with recent observations [49], ROS generation is caspase-dependent in glioma cells, as shown by near-complete blocking of this process using Z-VAD-fmk.

Our study also demonstrated that vorinostat/bortezomib-induced apoptosis depends on the upregulation of Noxa and Bim, and cleavage of Mcl-1, which promotes the disturbance of mitochondrial membrane potential resulting in activation of the intrinsic apoptosis pathway. BH3-only proteins are known to be the sensors that mediate apoptotic signals and mitochondrial depolarization, although it is not entirely clear how BH3-only proteins activate the apoptotic machinery. It has been proposed that they may block the antiapoptotic effect of members of the Bcl-2 superfamily, and/or induce Bax/Bak conformational change [50]. The observations that activation of both Bax and Bak and their conformational changes are involved in bortezomib/vorinostat-induced apoptosis suggest that modulation of Bcl-2 family homeosta-sis represents a major contributing factor in the initiation of apoptotic

signals by the inhibitors. These findings are also consistent with observations by Giuliano et al. [26] that Bax activation is a putative mediator of apoptotic signaling in this context. Once activated, these BH3-only proteins (such as Bid, Bim, and Noxa) are free to interact with multi-domain BH proteins that reside at the outer mitochondrial membrane and can activate Bax and Bak, and facilitate the formation of megachannels in the outer mitochondrial membrane, thus allowing the release of cytochrome *c* and other apoptogenic factors, such as Smac/DIA-BLO, from mitochondria.

Among the Bcl-2 family of proteins, bortezomib and HDACI treatment resulted in the accumulation of Mcl-1 and its cleaved form, as well as increased amounts of Noxa. Although Noxa was initially reported as being directly regulated by p53, several studies have shown p53-independent induction of Noxa following exposure to PIs or HDACIs [51,52]. In agreement with these studies, we confirmed upregulation of Noxa in a p53-mutant cell line (T98G), which suggested that Noxa expression occurs in a p53-independent manner in human glioma. It has been shown that Noxa binds to Mcl-1 proteins and is also capable of displacing proapoptotic Bak from Mcl-1 [39]. Our results show that treatment of glioma cells with bortezomib/vorinostat triggers Noxa induction and the majority of this protein binds to Mcl-1. In addition, this coupling allows Bak to be released from Mcl-1. Once liberated, Bak may induce mitochondrial dysfunction. The mechanism whereby bortezomib and vorinostat increase Noxa expression is beyond the scope of the current manuscript, although some reports demonstrate that increased expression is clearly due to an upregulation of mRNA for Noxa [53]. Our results agree with previously published observations [52,53] that bortezomib-induced apoptosis was associated with Mcl-1 cleavage. Moreover, exposure of glioma cells to vorinostat and bortezomib resulted in a clear increase in expression of Bim. After bortezomib and vorinostat treatment, Mcl-1/Bim complexes were barely detectable (BimL and BimS), revealing the disruption of Mcl-1/Bim complexes which could promote apoptosis by directly activating multido-main proapoptotic molecules Bax/Bak, by antagonizing the antiapoptotic actions of Bcl-2 and Bcl-xL, or by a combination of these actions [50,54–56]. Recently Han et al. [57] have demonstrated that Mcl-1 is a direct substrate for caspase-8, and that loss of Mcl-1 generates Mcl-1-free Bim that is involved in the ensuing apoptotic events, suggesting the potential existence of a novel crosstalk mechanism between the extrinsic and the intrinsic apoptotic pathways to initiate apoptosis. We have also shown that Noxa and Mcl-1 play a major role in mediating the synergistic effects of vorinostat + bortezomib. It is noteworthy that Noxa is known to bind with high affinity to Mcl-1 [38]. This suggests that Noxa upregulation in response to vorinostat and bortezomib may serve to functionally inactivate Mcl-1, causing displacement of proapoptotic proteins bound to the Mcl-1 protein. Together, the bortezomib/vorinostat regimen may trigger cell death through multiple interacting mechanisms, including disabling the cytoprotective Bcl-2 family proteins in glioma cells.

We have shown that exposure to vorinostat, alone [10] or in combination with bortezomib (unpublished observation, data not shown), promotes histone acetylation. The resulting chromosomal relaxation may render DNA more sensitive to lethal injury as a promoter or consequence of apoptotic signaling. As a sensitive oxidative DNA damage marker, the striking increases of H2AX phosphorylation that were observed after combined vorinostat

and bortezomib treatment imply the promotion of DNA double-strand break formation by the combination, which may play an important role in the synergistic enhancement of DNA damage and apoptosis. An additional mechanism for the synergy may be due to abrogation of DNA double-strand break repair mediated by Rad51 repression. The fact that combination of bortezomib with vorinostat markedly enhanced both the accumulation of γH2AX and loss of RAD51 may in part explain the dramatic sensitizing effect of this combination in human glioma cells. These results raise the possibility of "multiple hits," one directly on the mitochondria to trigger apoptosis and the other in the cell nucleus, resulting in DNA damage, cell cycle arrest, and impaired DNA repair, which may combine to make the combination of bortezomib and vorinostat highly efficient in killing glioma cells.

In sum, our results demonstrate that co-treatment with vorinostat and bortezomib activates the intrinsic (mitochondria-dependent) apoptotic pathway in malignant human glioma cells. This is based on several pieces of evidence: (1) induction of cytochrome *c* release; (2) loss of mitochondrial membrane potential; (3) increased generation of ROS; (4) modulation of the Bcl-2 family proteins; and (5) induction of DNA damage, which influences the synergistic potentiation of apoptosis signaling. Taken together, these observations provide a strong rationale for combining vorinostat with bortezomib in clinical applications for patients with glioma.

Supplementary Material

Refer to Web version on PubMed Central for supplementary material.

Acknowledgments

The authors thank Robert Lacomy and Alexis Styche for technical assistance. This work was supported by National Institutes of Health Grant P01NS40923 (I.F.P.) and by The Walter L. Cope-land Fund of the Pittsburgh Foundation (D.R.P.).

Abbreviations

HDACIs	histone deacetylase inhibitors
PIs	proteasome inhibitors
GBM	glioblastoma multiforme
NHA	normal human astrocytes
NAC	*N*-acetyl-L-cysteine
PBS	phosphate-buffered saline
ROS	reactive oxygen species
H_2DCFDA	2′,7′-dichloro-dihydrofluorescein diacetate
TBS	Tris-buffered saline
NHA	non-neoplastic human astrocytes

References

1. Omuro AM, Faivre S, Raymond E. Lessons learned in the development of targeted therapy for malignant gliomas. Mol Cancer Ther. 2007; 6:1909–1919. [PubMed: 17620423]
2. Wolffe AP, Guschin D. Review: Chromatin structural features and targets that regulate transcription. J Struct Biol. 2000; 129:102–122. [PubMed: 10806063]
3. Marks P, Rifkind RA, Richon VM, Breslow R, Miller T, Kelly WK. Histone deacetylases and cancer: Causes and therapies. Nat Rev Cancer. 2001; 1:194–202. [PubMed: 11902574]
4. Ruefli AA, Ausserlechner MJ, Bernhard D, et al. The histone deacetylase inhibitor and chemotherapeutic agent suberoylanilide hydroxamic acid (SAHA) induces a cell-death pathway characterized by cleavage of Bid and production of reactive oxygen species. Proc Natl Acad Sci USA. 2001; 98:10833–10838. [PubMed: 11535817]
5. Burgess A, Ruefli A, Beamish H, et al. Histone deacetylase inhibitors specifically kill nonproliferating tumour cells. Oncogene. 2004; 23:6693–6701. [PubMed: 15235588]
6. Rao R, Fiskus W, Yang Y, et al. HDAC6 inhibition enhances 17-AAG-mediated abrogation of hsp90 chaperone function in human leukemia cells. Blood. 2008; 112:1886–1893. [PubMed: 18591380]
7. Marks PA, Breslow R. Dimethyl sulfoxide to vorinostat: Development of this histone deacetylase inhibitor as an anticancer drug. Nat Biotechnol. 2007; 25:84–90. [PubMed: 17211407]
8. Lucas DM, Davis ME, Parthun MR, et al. The histone deacetylase inhibitor MS-275 induces caspase-dependent apoptosis in B-cell chronic lymphocytic leukemia cells. Leukemia. 2004; 18:1207–1214. [PubMed: 15116122]
9. Finnin MS, Donigian JR, Cohen A, et al. Structures of a histone deacetylase homologue bound to the TSA and SAHA inhibitors. Nature. 1999; 401:188–193. [PubMed: 10490031]
10. Jane EP, Premkumar DR, Addo-Yobo SO, Pollack IF. Abrogation of mitogen-activated protein kinase and Akt signaling by vandetanib synergistically potentiates histone deacetylase inhibitor-induced apoptosis in human glioma cells. J Pharmacol Exp Ther. 2009; 331:327–337. [PubMed: 19622715]
11. Wetzel M, Premkumar DR, Arnold B, Pollack IF. Effect of trichostatin A, a histone deacetylase inhibitor, on glioma proliferation in vitro by inducing cell cycle arrest and apoptosis. J Neurosurg. 2005; 103:549–556. [PubMed: 16383255]
12. Yin D, Ong JM, Hu J, et al. Suberoylanilide hydroxamic acid, a histone deacetylase inhibitor: Effects on gene expression and growth of glioma cells in vitro and in vivo. Clin Cancer Res. 2007; 13:1045–1052. [PubMed: 17289901]
13. Ugur HC, Ramakrishna N, Bello L, et al. Continuous intracranial administration of suberoylanilide hydroxamic acid (SAHA) inhibits tumor growth in an orthotopic glioma model. J Neurooncol. 2007; 83:267–275. [PubMed: 17310267]
14. Adams J. The proteasome: A suitable antineoplastic target. Nat Rev Cancer. 2004; 4:349–360. [PubMed: 15122206]
15. Richardson PG, Barlogie B, Berenson J, et al. Clinical factors predictive of outcome with bortezomib in patients with relapsed, refractory multiple myeloma. Blood. 2005; 106:2977–2981. [PubMed: 16020506]
16. Jane EP, Premkumar DR, Pollack IF. Bortezomib sensitizes malignant human glioma cells to TRAIL, mediated by inhibition of the NF-{kappa}B signaling pathway. Mol Cancer Ther. 2011; 10:198–208. [PubMed: 21220502]
17. Aghajanian C, Soignet S, Dizon DS, et al. A phase I trial of the novel proteasome inhibitor PS341 in advanced solid tumor malignancies. Clin Cancer Res. 2002; 8:2505–2511. [PubMed: 12171876]
18. Papandreou CN, Daliani DD, Nix D, et al. Phase I trial of the proteasome inhibitor bortezomib in patients with advanced solid tumors with observations in androgen-independent prostate cancer. J Clin Oncol. 2004; 22:2108–2121. [PubMed: 15169797]
19. Marcus AI, Zhou J, O'Brate A, et al. The synergistic combination of the farnesyl transferase inhibitor lonafarnib and paclitaxel enhances tubulin acetylation and requires a functional tubulin deacetylase. Cancer Res. 2005; 65:3883–3893. [PubMed: 15867388]

20. Riss TL, Moravec RA. Comparison of MTT, XTT and a novel tetrazolium compound MTS for in vitro proliferation and chemosensitivity assays. Mol Biol Cell. 1992; 3:184.
21. Jane EP, Premkumar DR, Pollack IF. AG490 influences UCN-01-induced cytotoxicity in glioma cells in a p53-dependent fashion, correlating with effects on BAX cleavage and BAD phosphorylation. Cancer Lett. 2007; 257:36–46. [PubMed: 17900801]
22. Nencioni A, Wille L, Dal Bello G, et al. Cooperative cytotoxicity of proteasome inhibitors and tumor necrosis factor-related apoptosis-inducing ligand in chemoresistant Bcl-2-overexpressing cells. Clin Cancer Res. 2005; 11:4259–4265. [PubMed: 15930365]
23. Nagy K, Szekely-Szuts K, Izeradjene K, et al. Proteasome inhibitors sensitize colon carcinoma cells to TRAIL-induced apoptosis via enhanced release of Smac/DIABLO from the mitochondria. Pathol Oncol Res. 2006; 12:133–142. [PubMed: 16998592]
24. Cossarizza A, Ferraresi R, Troiano L, et al. Simultaneous analysis of reactive oxygen species and reduced glutathi-one content in living cells by polychromatic flow cytometry. Nat Protoc. 2009; 4:1790–1797. [PubMed: 20010930]
25. Chou TC, Talalay P. Quantitative analysis of dose-effect relationships: The combined effects of multiple drugs or enzyme inhibitors. Adv Enzyme Regul. 1984; 22:27–55. [PubMed: 6382953]
26. Giuliano M, Lauricella M, Calvaruso G, et al. The apoptotic effects and synergistic interaction of sodium butyrate and MG132 in human retinoblastoma Y79 cells. Cancer Res. 1999; 59:5586–5595. [PubMed: 10554039]
27. Pei XY, Dai Y, Grant S. Synergistic induction of oxidative injury and apoptosis in human multiple myeloma cells by the proteasome inhibitor bortezomib and histone deacetylase inhibitors. Clin Cancer Res. 2004; 10:3839–3852. [PubMed: 15173093]
28. Heider U, von Metzler I, Kaiser M, et al. Synergistic interaction of the histone deacetylase inhibitor SAHA with the proteasome inhibitor bortezomib in mantle cell lymphoma. Eur J Haematol. 2008; 80:133–142. [PubMed: 18005386]
29. Rosato RR, Almenara JA, Grant S. The histone deacetylase inhibitor MS-275 promotes differentiation or apoptosis in human leukemia cells through a process regulated by generation of reactive oxygen species and induction of p21CIP1/WAF1 1. Cancer Res. 2003; 63:3637–3645. [PubMed: 12839953]
30. Miller CP, Ban K, Dujka ME, et al. NPI-0052, a novel proteasome inhibitor, induces caspase-8 and ROS-dependent apoptosis alone and in combination with HDAC inhibitors in leukemia cells. Blood. 2007; 110:267–277. [PubMed: 17356134]
31. Zheng Y, Yamaguchi H, Tian C, et al. Arsenic trioxide (As(2)O(3)) induces apoptosis through activation of Bax in hematopoietic cells. Oncogene. 2005; 24:3339–3347. [PubMed: 15735709]
32. Ling YH, Lin R, Perez-Soler R. Erlotinib induces mitochondrial-mediated apoptosis in human H3255 non-small-cell lung cancer cells with epidermal growth factor receptorL858R mutation through mitochondrial oxidative phosphorylation-dependent activation of BAX and BAK. Mol Pharmacol. 2008; 74:793–806. [PubMed: 18524889]
33. Premkumar DR, Jane EP, Pollack IF. Co-administration of NVP-AEW541 and dasatinib induces mitochondrial-mediated apoptosis through Bax activation in malignant human glioma cell lines. Int J Oncol. 2010; 37:633–643. [PubMed: 20664932]
34. George NM, Evans JJ, Luo X. A three-helix homo-oligomerization domain containing BH3 and BH1 is responsible for the apoptotic activity of Bax. Genes Dev. 2007; 21:1937–1948. [PubMed: 17671092]
35. Vander Heiden MG, Chandel NS, Williamson EK, Schumacker PT, Thompson CB. Bcl-xL regulates the membrane potential and volume homeostasis of mitochondria. Cell. 1997; 91:627–637. [PubMed: 9393856]
36. Marzo I, Susin SA, Petit PX, et al. Caspases disrupt mitochondrial membrane barrier function. FEBS Lett. 1998; 427:198–202. [PubMed: 9607311]
37. Lalier L, Cartron PF, Juin P, et al. Bax activation and mitochondrial insertion during apoptosis. Apoptosis. 2007; 12:887–896. [PubMed: 17453158]
38. Chen L, Willis SN, Wei A, et al. Differential targeting of prosurvival Bcl-2 proteins by their BH3-only ligands allows complementary apoptotic function. Mol Cell. 2005; 17:393–403. [PubMed: 15694340]

39. Willis SN, Chen L, Dewson G, et al. Proapoptotic Bak is sequestered by Mcl-1 and Bcl-xL, but not Bcl-2, until displaced by BH3-only proteins. Genes Dev. 2005; 19:1294–1305. [PubMed: 15901672]
40. Golding SE, Rosenberg E, Khalil A, et al. Double strand break repair by homologous recombination is regulated by cell cycle-independent signaling via ATM in human glioma cells. J Biol Chem. 2004; 279:15402–15410. [PubMed: 14744854]
41. Ohnishi T, Taki T, Hiraga S, Arita N, Morita T. In vitro and in vivo potentiation of radiosensitivity of malignant gliomas by antisense inhibition of the RAD51 gene. Biochem Biophys Res Commun. 1998; 245:319–324. [PubMed: 9571148]
42. Russell JS, Brady K, Burgan WE, et al. Gleevec-mediated inhibition of Rad51 expression and enhancement of tumor cell radiosensitivity. Cancer Res. 2003; 63:7377–7383. [PubMed: 14612536]
43. Chinnaiyan P, Vallabhaneni G, Armstrong E, Huang SM, Harari PM. Modulation of radiation response by histone deacetylase inhibition. Int J Radiat Oncol Biol Phys. 2005; 62:223–229. [PubMed: 15850925]
44. Rogakou EP, Pilch DR, Orr AH, Ivanova VS, Bonner WM. DNA double-stranded breaks induce histone H2AX phosphorylation on serine 139. J Biol Chem. 1998; 273:5858–5868. [PubMed: 9488723]
45. Al-Janadi A, Chandana SR, Conley BA. Histone deacetylation: An attractive target for cancer therapy? Drugs R D. 2008; 9:369–383. [PubMed: 18989989]
46. Galanis E, Jaeckle KA, Maurer MJ, et al. Phase II trial of vorinostat in recurrent glioblastoma multiforme: A north central cancer treatment group study. J Clin Oncol. 2009; 27:2052–2058. [PubMed: 19307505]
47. Thaker NG, Zhang F, McDonald PR, et al. Identification of survival genes in human glioblastoma cells by small interfering RNA screening. Mol Pharmacol. 2009; 76:1246–1255. [PubMed: 19783622]
48. Weller M, Rieger J, Grimmel C, et al. Predicting chemoresistance in human malignant glioma cells: The role of molecular genetic analyses. Int J Cancer. 1998; 79:640–644. [PubMed: 9842975]
49. Sanchez Y, Simon GP, Calvino E, de Blas E, Aller P. Curcumin stimulates reactive oxygen species production and potentiates apoptosis induction by the antitumor drugs arsenic trioxide and lonidamine in human myeloid leukemia cell lines. J Pharmacol Exp Ther. 2010; 335:114–123. [PubMed: 20605902]
50. Letai A, Bassik MC, Walensky LD, Sorcinelli MD, Weiler S, Korsmeyer SJ. Distinct BH3 domains either sensitize or activate mitochondrial apoptosis, serving as prototype cancer therapeutics. Cancer Cell. 2002; 2:183–192. [PubMed: 12242151]
51. Inoue S, Riley J, Gant TW, Dyer MJ, Cohen GM. Apoptosis induced by histone deacetylase inhibitors in leukemic cells is mediated by Bim and Noxa. Leukemia. 2007; 21:1773–1782. [PubMed: 17525724]
52. Perez-Galan P, Roue G, Villamor N, Montserrat E, Campo E, Colomer D. The proteasome inhibitor bortezomib induces apoptosis in mantle-cell lymphoma through generation of ROS and Noxa activation independent of p53 status. Blood. 2006; 107:257–264. [PubMed: 16166592]
53. Gomez-Bougie P, Wuilleme-Toumi S, Menoret E, et al. Noxa up-regulation and Mcl-1 cleavage are associated to apoptosis induction by bortezomib in multiple myeloma. Cancer Res. 2007; 67:5418–5424. [PubMed: 17545623]
54. Green DR. At the gates of death. Cancer Cell. 2006; 9:328–330. [PubMed: 16697952]
55. Kuwana T, Bouchier-Hayes L, Chipuk JE, et al. BH3 domains of BH3-only proteins differentially regulate Bax-mediated mitochondrial membrane permeabilization both directly and indirectly. Mol Cell. 2005; 17:525–535. [PubMed: 15721256]
56. Willis SN, Fletcher JI, Kaufmann T, et al. Apoptosis initiated when BH3 ligands engage multiple Bcl-2 homologs, not Bax or Bak. Science. 2007; 315:856–859. [PubMed: 17289999]
57. Han J, Goldstein LA, Gastman BR, Rabinovitz A, Rabinowich H. Disruption of Mcl-1. Bim complex in granzyme B-mediated mitochondrial apoptosis. J Biol Chem. 2005; 280:16383–16392. [PubMed: 15713684]

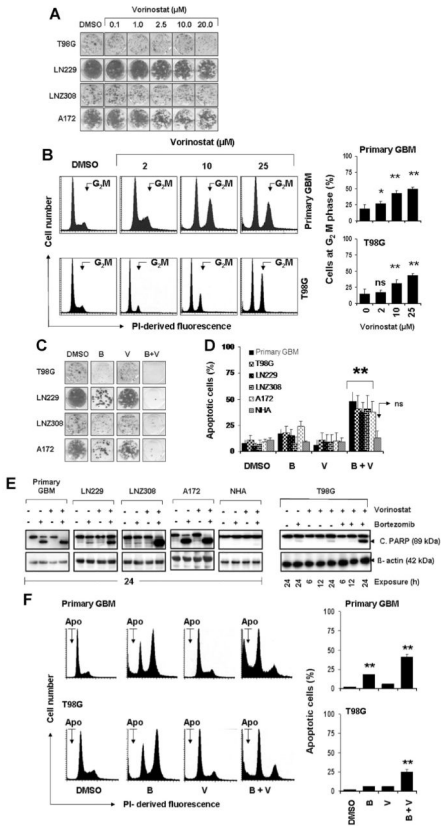

Figure 1.

Bortezomib sensitizes glioma cells to vorinostat. (A) T98G, LN229, LNZ308, and A172 cells were exposed to the indicated concentrations of vorinostat for 24 h. On the following day, the media were changed and complete media were added and cells were grown for additional 14 d in the absence of inhibitors. Control cells received equivalent concentrations of vehicle, DMSO. Colonies were fixed and stained as described in the Materials and Methods Section. (B) Analysis of cell cycle distribution and frequency of cells at G_2M phase by vorinostat in primary GBM and T98G cells. Cells were seeded at 60% confluence, allowed to attach overnight, and treated with the indicated concentrations of vorinostat for 24 h. Cell cycle analysis using propidium iodide (PI) staining was performed as described in the Materials and Methods Section. Representative DNA profile (left) and the cells at G_2M phase from three independent experiments shown at the right. Asterisks indicate significant differences in relation to untreated control ($^{*}P < 0.05$; $^{**}P < 0.005$; ns, not significant). (C) T98G, LN229, LNZ308, and A172 cells were treated with bortezomib (5 nM, B) or vorinostat (2 μM, V) or the combination of bortezomib plus vorinostat (B + V) for 24 h. Control cells received DMSO. Clonogenic assay was performed as described in the Materials and Methods Section. (D) Glioma (primary GBM, T98G, LN229, LNZ308, and A172) and normal human astrocytes (NHA) were treated as described in “C” and frequency of apoptotic cells was determined by cell surface annexin V binding assay. The results represent the mean ± SD of at least three different experiments. Asterisks indicate significant differences in relation to untreated control. $^{**}P < 0.005$; ns, not significant. (E) Primary tumor cells (primary GBM), established human glioma cell lines (LN229, LNZ308,

A172, and T98G) and non-neoplastic normal human astrocytes (NHA) were treated as described in “C” for the indicated durations. Cell extracts were prepared, and equal amounts of protein were separated by SDS–PAGE and subjected to Western blotting analysis with anti-PARP antibody. β-actin served as loading control. (F) Left, representative DNA profile (Apo, cells at sub-G_1) and the bar chart (indicating sub-G_1, apoptotic cells; mean ± SD, right) from three independent experiments of primary GBM and T98G cell line treated as “C.” Asterisks indicate significant differences in relation to untreated control ($^{**}P < 0.005$).

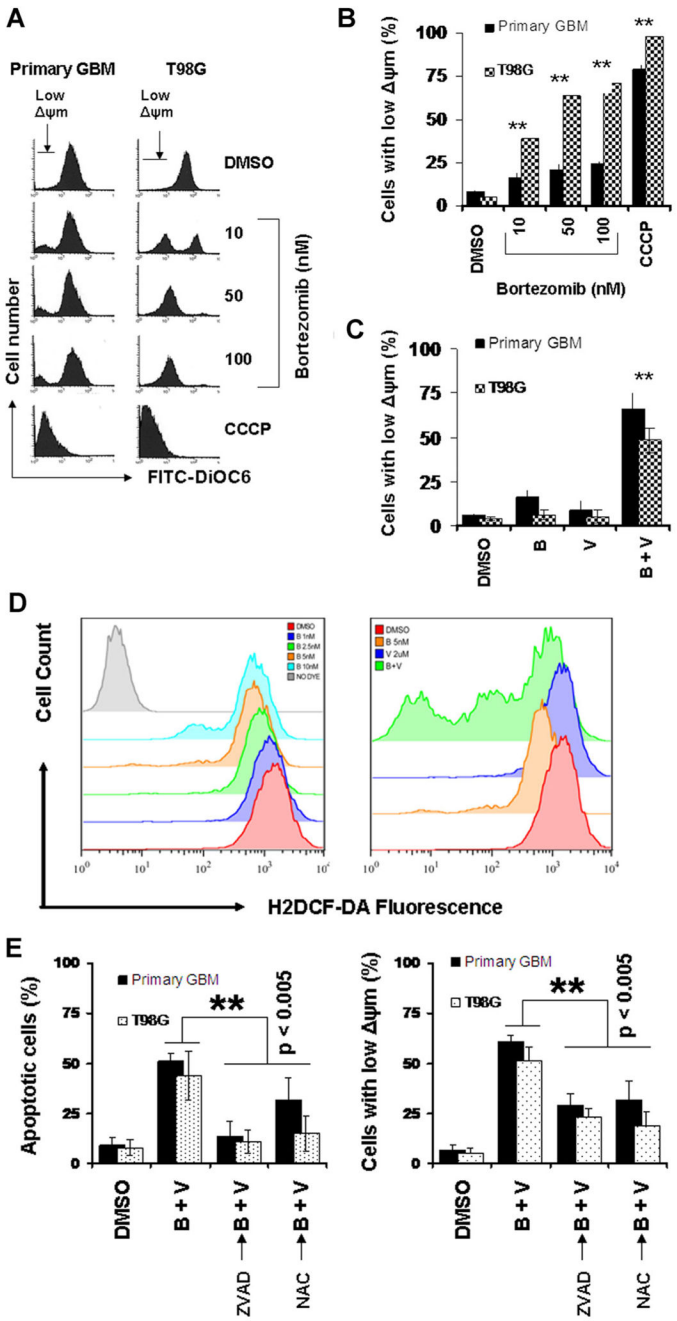

Figure 2.

Combination of bortezomib and vorinostat induces loss of mitochondrial potential and release of ROS, and activates the intrinsic apoptotic pathway. (A and B) Primary tumor cells (primary GBM) and T98G cell line were treated with the indicated concentrations of bortezomib for 24 h. Control cells received equivalent amount of DMSO. Cells were then loaded with DiOC6 and mitochondrial membrane potential was analyzed by flow cytometry as described in the Materials and Methods Section. CCCP served as positive control (50 μM). Note the appearance of a subpopulation of cells with decreased fluorescence (cells with low $\Delta\psi_m$) in a dose-dependent manner (A). Bar chart represents the cells with low $\Delta\psi_m$

(mean ± SD) from three independent experiments (B). Asterisks indicate significant differences in relation to untreated control ($^{**}P < 0.005$). (C) Primary tumor cells and T98G cell line were treated with bortezomib (5 nM), vorinostat (2 μM) or the combination of bortezomib plus vorinostat (B + V) for 24 h. Loss of mitochondrial membrane potential was determined by DiOC6 staining and flow cytometry. (D) Analysis of ROS generation by H2DCF-DA staining and flow cytometry. Primary tumor cells were exposed to the indicated concentration of bortezomib (left). Increasing the dose of bortezomib resulted in a decrease in the H2DCF-DA fluorescence intensity. Co-treating cells with bortezomib + vorinostat (B + V; bortezomib 5 nM + vorinostat 2 μM) for 24 h provoked much lower H2DCF-DA fluorescence intensity than the single agent alone (right). (E) Primary tumor and T98G cells were pretreated with 25 μM ZVAD-fmk (pan caspase inhibitor) or 5 mM NAC (ROS scavenger) for 2 h followed by the combination of bortezomib (5 nM) plus vorinostat (2 μM, B + V) for 24 h. Control cells received equivalent amount of DMSO. Apoptosis (annexin V binding, left) and loss of mitochondrial membrane potential ($\Delta\psi_m$, DiOC6 assay, right) was analyzed by flow cytometry as described in the Materials and Methods Section. Data are representative of triplicate in three independent experiments ($^{**}P < 0.005$).

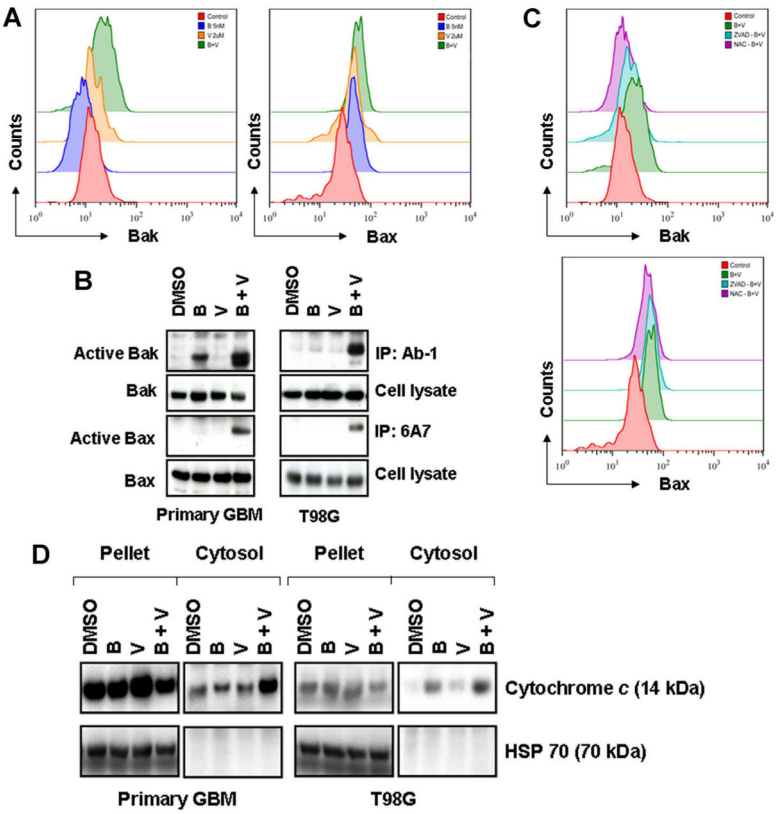

Figure 3.

Co-treatment with bortezomib and vorinostat induces Bak and Bax conformational changes and cytochrome *c* release. (A) Representative histograms of Bak and Bax conformational changes in cells treated with bortezomib or vorinostat or the combination of both are presented. T98G cells were treated with bortezomib (5 nM) or vorinostat (2 μM) or the combination of both for 24 h. After treatment, cells were fixed with formaldehyde and then incubated with 6A7 monoclonal anti-Bax antibody or with monoclonal anti-Bak (Ab1) antibody. After incubation with FITC-conjugated secondary antibody for 2 h, the signals of activated conformation of Bax and Bak proteins were measured by flow cytometry. Data are representative of three independent experiments. (B) Vorinostat and bortezomib-induced Bak and Bax activation was validated by immunoprecipitation and Western blot analysis. Primary tumor and T98G cells were treated as described in "A." After treatment with inhibitors, cells were harvested, lysed and equal amounts of protein were immunoprecipitated (IP) with Ab1 anti-Bak or 6A7 anti-Bax antibody and probed with polyclonal anti-Bak or anti-Bax, respectively. In parallel, the total amounts of Bak and Bax were detected by immunoblot using polyclonal anti-Bak and anti-Bax antibody. (C) T98G cells were pretreated with 25 μM ZVAD-fmk (pan caspase inhibitor) or 5 mM NAC (ROS scavenger) for 2 h followed by the combination of bortezomib (5 nM) plus vorinostat (2 μM, B + V) for 24 h. Control cells received an equivalent amount of DMSO. Bak (upper panel) and Bax (lower panel) activation were measured by flow cytometry as described in the Materials and Methods Section. (D) Primary GBM and T98G cells were incubated with inhibitors as described in "A." Cytosolic extracts and the digitonin-insoluble pellet were

prepared as described in the Materials and Methods Section. Equal amounts of protein were separated by SDS–PAGE and subjected to Western blotting analysis with cytochrome *c* and heat shock protein 70 (HSP70) antibodies, respectively. The distribution of HSP70 was used to determine that cytoplasmic cytochrome *c* did not result from mitochondria damaged in the course of the protocol.

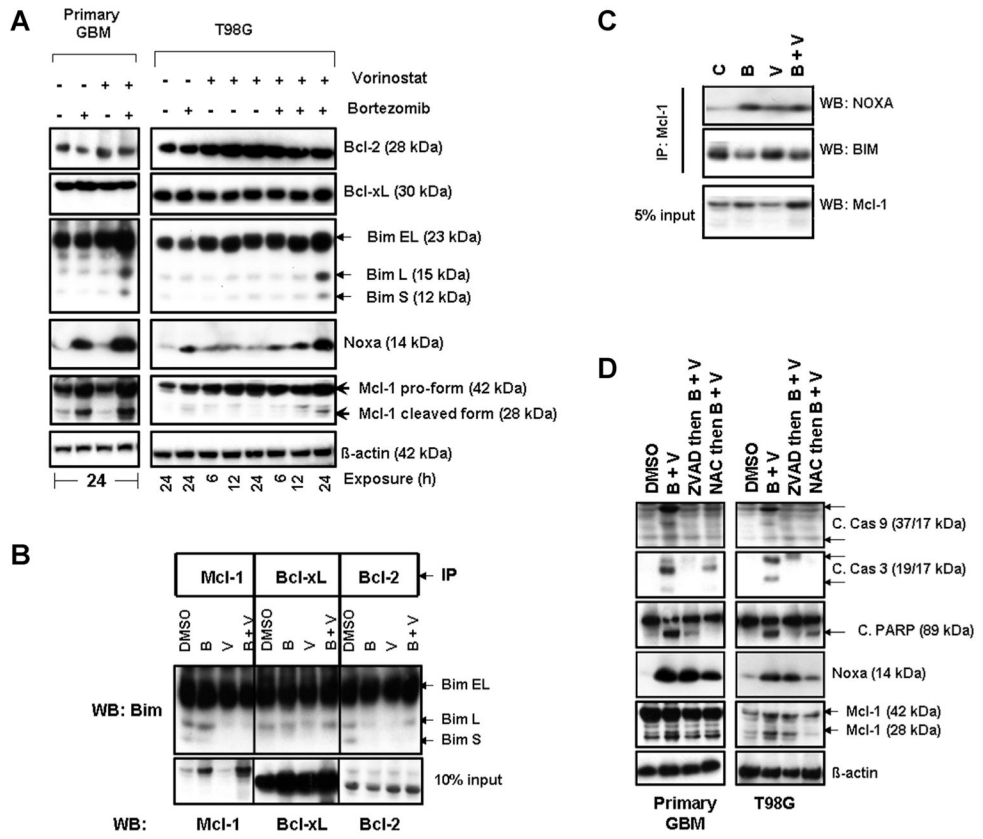

Figure 4.

Co-treatment with bortezomib and vorinostat induces Noxa, disrupts Mcl1/Bim complexes, and activates Bak and Bax. (A) Primary tumor and T98G cells were treated with bortezomib (5 nM) or vorinostat (2 μM) or the combination for the durations noted. Cell extracts were prepared, and equal amounts of protein were separated by SDS–PAGE and subjected to Western blotting analysis with the indicated antibodies. β-actin served as loading control. (B) T98G cells were treated with inhibitors for 24 h. An equal amount of protein was immunoprecipitated (IP) with the indicated antibodies as described in the Materials and Methods Section. Immunoprecipitates were subjected to Western blot (WB) analysis using anti-Bim antibody. Samples of whole cell lysates (WCL) were subjected to Western blot analysis to monitor the total levels of the respective proteins. (C) T98G cells were treated with inhibitors for 24 h as described in "A." To assess the association of Mcl-1 and Noxa or Bim, immunoprecipitation (IP) was performed using Mcl-1 antibody. Immunoprecipitates were subjected to Western blot (WB) analysis. Samples of whole cell lysates (WCL) were subjected to Western blot analysis to monitor the total levels of Mcl-1. (D) Primary tumor and T98G cells were pretreated with 25 μM ZVAD-fmk (pan caspase inhibitor) or 5 mM NAC (ROS scavenger) for 2 h followed by the combination of bortezomib (5 nM) plus vorinostat (2 μM, B + V) for 24 h. Control cells received an equivalent amount of DMSO. Western blot analysis was performed with the indicated antibodies. β-actin served as loading control.

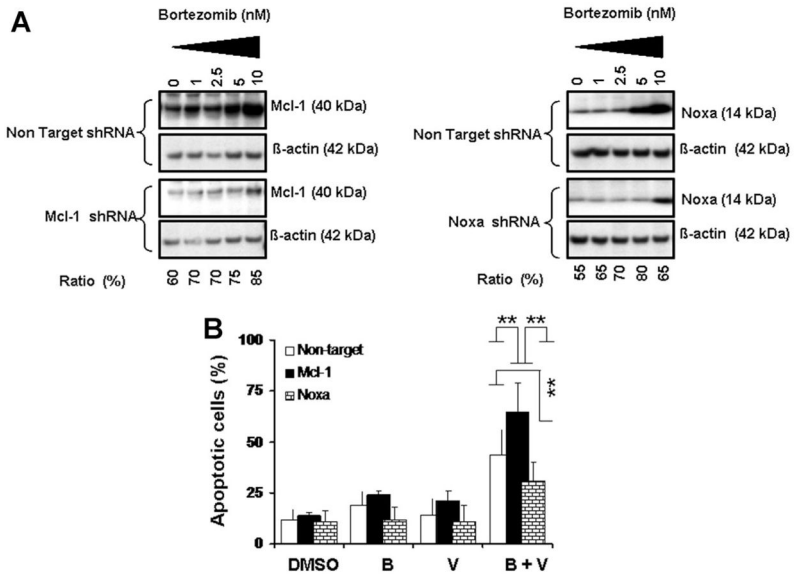

Figure 5.

Knocking down Mcl-1 expression increases glioma cell sensitivity to bortezomib and vorinostat and knocking down Noxa expression protects cells from killing induced by the combination of bortezomib and vorinostat. (A) T98G cells were transfected with non-target or Mcl-1 or Noxa shRNA as described in the Materials and Methods Section. Forty-eight hours posttransfection, cells were treated with the indicated concentrations of bortezomib for 24 h. Lysates were collected and protein was subjected to Western blot analysis using anti-Mcl-1 (left panel) or anti-Noxa (right panel) antibodies. Blots were stripped and reprobed with β-actin. Densitometric analysis of the band intensity was measured, and the numbers below the blot represent percent inhibition of protein in relation to the corresponding control (non-target shRNA). (B) T98G cells were transiently transfected with non-target or Mcl-1 or Noxa shRNA as described in the Materials and Methods Section. After 48 h posttransfection cells were exposed to bortezomib (5 nM) with or without vorinostat (2 μM) for 24 h and cell viability was assessed by annexin V apoptosis assay. Control cells received vehicle (DMSO). Data are representative of triplicate in three independent experiments ($^{**}P < 0.005$).

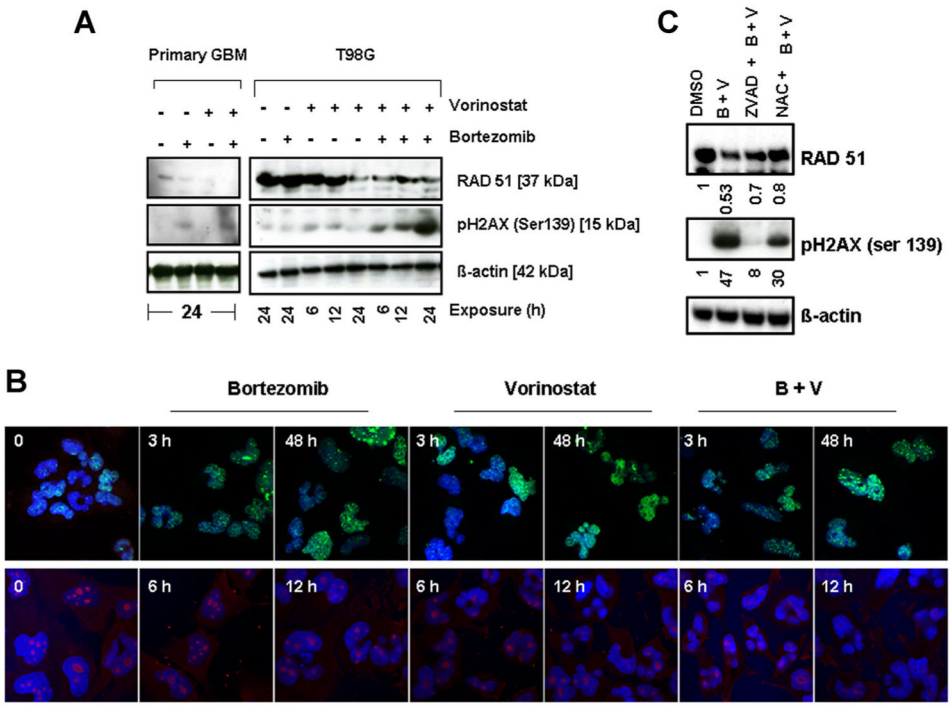

Figure 6.

Vorinostat and bortezomib provoke DNA damage response in malignant human glioma cell lines. (A) Primary tumor and T98G cells were treated with bortezomib (5 nM) or vorinostat (2 μM) or the combination for the indicated duration. Cell extracts were prepared, and equal amounts of protein were separated by SDS–PAGE and subjected to Western blotting analysis with the indicated antibodies. β-actin served as the loading control. (B) T98G cells were exposed to bortezomib or vorinostat or the combination of both for the indicated duration. Cells were stained with antibodies to phospho-γH2AX (1:50 dilution) (upper panel) and RAD51 (1:100 dilution) (lower panel). Nuclei were stained blue with Hoechst. Control cells (O) received DMSO. (C) T98G cells were pre-treated with 25 μM ZVAD-fmk (pan caspase inhibitor) or 5 mM NAC (ROS scavenger) for 2 h followed by the combination of bortezomib (5 nM) plus vorinostat (2 μM, B + V) for 24 h. Control cells received equivalent amounts of DMSO. Western blotting analysis was performed with the indicated antibodies. β-actin served as loading control. Densitometric analysis of the band intensity was measured and the numbers below the blot represent the fold difference compared to untreated control (DMSO).